

Understanding doping effects on P2 $\text{Na}_x\text{Mn}_{1-y}\text{M}_y\text{O}_2$ ($M = \text{Li, Mg, Al, Ti, V, Cr, Fe, Co, Ni}$) cathode materials for Na-ion batteries

Huu Duc Luong 


*Department of Precision Science & Technology and Applied Physics, Graduate School of Engineering,
Osaka University, Suita, Osaka 565-0871, Japan
and Department of Theoretical Nanotechnology, Institute of Scientific and Industrial Research,
Osaka University, Ibaraki, Osaka 567-0047, Japan*

Hiroyoshi Momida 

*Institute of Scientific and Industrial Research, Osaka University, Ibaraki, Osaka 567-0047, Japan
and Elements Strategy Initiative for Catalysts and Batteries, Kyoto University, Kyoto 615-8245, Japan*

Van An Dinh *

*Institute of Applied Technology, Thu Dau Mot University, Binh Duong Province 820000, Vietnam
and Department of Precision Engineering, Graduate School of Engineering, Osaka University, Suita, Osaka 565-0871, Japan*

Tamio Oguchi †

*Elements Strategy Initiative for Catalysts and Batteries, Kyoto University, Kyoto 615-8245, Japan
and Center for Spintronics Research Network, Osaka University, Toyonaka, Osaka 560-8531, Japan*



(Received 27 September 2021; revised 8 January 2022; accepted 11 January 2022; published 24 January 2022)

The P2-layered oxide NaMnO_2 is known as a cheap and high-capacity material for secondary batteries, but has been limited in application due to the large Jahn-Teller lattice distortion. Through the highly accurate hybrid functional method (HSE06), we computationally evaluate the doping influences on the lattice distortions, stabilities, electronic structures, redox potentials, and diffusion mechanisms. Our calculations indicate that dopants not only reduce the lattice distortion degree, especially for Li, Mg, Ti, and V cases, but also increase the stability of the structure, implying the dopants would alleviate the Jahn-Teller lattice distortion. At low Na concentrations, the Li dopant preferably diffuses out of the MnO_2 layer, but hardly moves to the Na layer, suggesting that P2-layered oxides can prevent the dopant's migrations during the Na extractions. At full Na concentrations, all the considered dopants, except for Ti and V, have a small effect on the redox potential. The effect on the diffusion mechanism is described through the diffusion of a Na ion-polaron complex near the dopant's environments. Fe, Mg, Ti, and Cr dopants can hinder the Na ion-polaron complex diffusion with significantly higher activation energies, respectively, while the Al dopant almost remains the activation energy as well as the perfect structure. However, Li, V, Co, and Ni dopants benefit from such complex diffusion with much lower activation energy so the ion diffusivities increase significantly. It is found that the doping influence on the activation energy for Na ion diffusion is associated with the $M\text{-O}$ bond change and charges of the neighboring dopants.

DOI: [10.1103/PhysRevMaterials.6.015802](https://doi.org/10.1103/PhysRevMaterials.6.015802)

I. INTRODUCTION

The carbon neutrality to eliminate carbon emission requires state-of-the-art technologies of electrical energy storage. A great endeavor has been made to improve the current rechargeable battery technology applied for portable devices and electric vehicles. Among the various battery technologies, Li-ion batteries (LIBs) have emerged as the highest achievement in the commercial energy storage market, which meets the requirements of lightweight, safety, and volumetric energy density. However, the ever-increasing energy demand

along with the scarcity of lithium in nature forces scientists to find the next generation of rechargeable batteries which not only exhibit similar or improved electrochemical properties but also require lower production costs and have long-term applications. Among the alternatives for the next generation of ion batteries, Na-based materials testing for rechargeable ion batteries shows similar properties as analogous Li-based compounds for LIBs. Particularly, Na compounds are much more abundant than lithium salts so their prices are 10 to 50 times cheaper than analogous materials of lithium [1]. As a result, Na-ion batteries (NIBs) have been anticipated to be the next generation of rechargeable batteries.

Among the promising cathode materials [2–17], the layered sodium manganese oxides are promising cathode materials for NIBs. Among several types of sodium manganese

*dinhvanan@tdmu.edu.vn

†oguchi@sanken.osaka-u.ac.jp

oxides, the P2 phase Na_xMnO_2 ($0 \leq x \leq 1$) exhibits a significantly higher capacity of 215 mAh/g and a voltage window of 2.0–3.5 V [18,19]. However, the samples show phase transformation due to the Jahn-Teller distortion during the intercalation and deintercalation. It causes the steplike plateaus to discharge a voltage line against the capacity. In our previous report [20], we demystified the deep insight into electrochemical properties of the P2-layered oxide. The Mn–O bond along the [010] direction could experience a large shrinkage/elongation so the material’s volume can change by up to 20% after all the Na ions are intercalated/deintercalated. It could be said that the large Jahn-Teller distortion is the direct culprit which limits the application of the auspicious cathode materials Na_xMnO_2 ($0 \leq x \leq 1$). In addition, the formed small polaron strongly binds and simultaneously accompanies the Na ion/vacancy so it generally impedes the diffusion of the Na ion/vacancy. The activation energy required for the Na vacancy–positive polaron complex [21] is 518 meV at rich Na ion regimes and reduces to 327 meV at low Na ion concentration.

Many endeavors have been devoted to remedying the electrochemical behaviors related to the structural degradation of the material upon cycling. A common strategy is doping other metals such as Li and Mg to Mn sites with different dopant concentrations $\text{Na}_x\text{Mn}_{1-y}M_y\text{O}_2$ ($M = \text{Li, Mg, } 0 \leq x \leq 1, \text{ and } y \leq 0.1$). In 2014, Billaud *et al.* [22] reported the doping effect of earth-abundant Mg with contents in the range from 0.05 to 0.1. The Mg-substituted samples exhibit a significantly smoother discharging voltage profile and a small reduction of the initial discharging capacity of 175 mAh/g when the Mg-substituted concentration increases. After that, Kwon *et al.* [23] doped Li to Mn sites with the dopant’s concentration in the range from 0.02 to 0.07. It was found that $\text{NaMn}_{0.93}\text{Li}_{0.07}\text{O}_2$ exhibits the smoothest voltage profile among various samples of different Li contents. However, a significant reduction in the distortion degree and lower discharge capacities were witnessed when Li content y increased from 0.02 to 0.07 because $3y$ Na ions would be immobile. Moreover, transition metal ions are alternatives to replace Mn sites to improve the electrochemical properties of this material. Kumakura *et al.* [24] reported the doping effect of five transition metals, including Ti, Co, Ni, Cu, and Zn of the M concentration of 0.1, on the distortion degree and electrochemical properties of the host materials. In general, the substitution of transition metals improves the electrochemical behaviors and reduces the lattice distortion degree.

Although improvement in electrochemical behaviors has been reported in the recent experimental progress, it is essential to comprehend the deep insight into the doping effect on the promising material. Zheng *et al.* [25] employed the *ab initio* molecular dynamics method to investigate the transition-metal (Fe, Co, Ni) mixing influence on kinetic properties of P2-layered oxide NaMnO_2 . However, the underestimated Na migration activation energies in the range from 46 meV to 100 meV due to the limitation of the calculation method suggests that a better simulation is vital to comprehend the doping effect on P2- NaMnO_2 . In the present paper, to continue our effort on promoting the electrochemical properties of P2-layered oxide phase Na_xMnO_2 , we conduct a

systematic investigation using the highly accurate hybrid functional method (HSE06) to analyze the influence of several cationic monovalent and multivalent dopants ($M = \text{Li, Mg, Al, Ti, V, Cr, Fe, Co, Ni}$) on the properties of the host material. The crystal structure, lattice distortion degree, thermodynamic stability, and electronic structure, together with the redox potential under the substitution of dopants to the Mn site are carefully addressed. Moreover, because the polaron formation cannot be neglected [21,26–34], the diffusion of the (Na ion–accompanying polaron) complex is also carefully investigated.

II. CALCULATION SCHEMES

All density functional theory calculations are accomplished by employing the VIENNA AB INITIO SIMULATION PACKAGE with projector augmented wave pseudo-potentials [35,36]. All spin-polarized calculations are performed using the hybrid functional method (HSE06) [37]. The supercell $4 \times 2 \times 1$ containing 32 formula units and a cutoff energy of 500 eV are used. To examine the effect of dopants on electrochemical properties of NaMnO_2 , a small dopant concentration of 0.07 to 0.1 has been reported to show a good influence on the electrochemical properties of substituted oxides [23,24]. Herein, we choose 0.0625 as the content of the dopants, which corresponds to two substituted M ions ($M = \text{Li, Mg, Al, Ti, V, Cr, Fe, Co, Ni}$) on the upper and lower layers of the $4 \times 2 \times 1$ supercell. The DFT functionals combined with the van der Waals (vdW-D3) correction may provide a better interpretation of the experimental observations [38]. Hence, we also employ the vdW-D3 correction scheme [39] in our HSE06 calculations. The structure optimizations are converged if the maximum residual atomic forces become less than $3 \times 10^{-2} \text{ eV \AA}^{-1}$. The diffusion mechanisms of Na ions near the dopant’s environment in the $4 \times 2 \times 1$ supercells are explored using the nudged elastic band (NEB) method [40]. The spring force between two images is set at -5 eV \AA^{-1} and the NEB calculations are converged if the NEB forces are smaller than $3 \times 10^{-2} \text{ eV \AA}^{-1}$.

III. RESULTS AND DISCUSSION

A. Effect on crystal structure

The crystal structures of doped P2-layered oxides $\text{NaMn}_{1-y}M_y\text{O}_2$ ($y = 1/16, M = \text{Li, Mg, Al, Ti, V, Cr, Fe, Co, and Ni}$) are shown in Fig. 1. In the crystal structure of NaMnO_2 , each Mn^{3+}O_6 octahedron (d^4) is surrounded by six adjacent Mn^{3+}O_6 octahedra, which can be divided into two groups. The first group (group 1NN) contains two Mn^{3+}O_6 octahedra along the [100] direction in which the Mn ions are the first-nearest neighbors at a distance of 2.91 Å. The second group (group 2NN) consists of four Mn^{3+}O_6 octahedra at a longer Mn–Mn distance of 3.20 Å.

When a Mn^{3+} ion is replaced by an alkali ion M^{m+} such as Li^+ or Mg^{2+} ions, the total number of electrons in the doped systems is $(3 - m)$ valence electrons less than that in the undoped structure. As a result, there are $(3 - m)$ Mn^{3+} ions oxidized to be Mn^{4+} . Our DFT calculations show that the oxidized Mn^{4+} ions prefer to locate at the 2NN sites with the lower energy differences (up to 720 meV for the Li case and

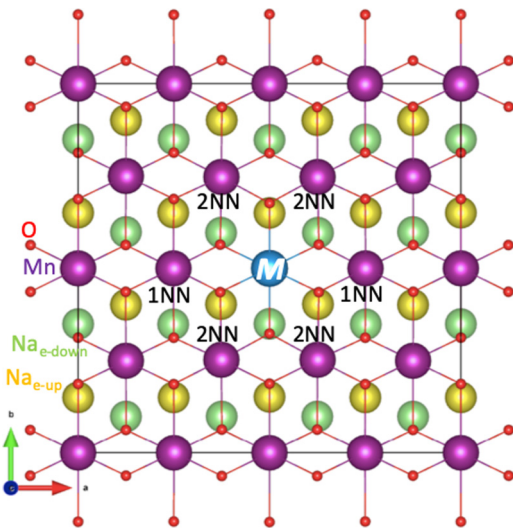


FIG. 1. Crystal structure of doped structure $\text{NaMn}_{1-y}\text{M}_y\text{O}_2$ ($y = 0.0625$, $M = \text{Li}, \text{Mg}, \text{Al}, \text{Ti}, \text{V}, \text{Cr}, \text{Fe}, \text{Co}$, and Ni) along c axis. Purple, red, blue, yellow, and green balls illustrate Mn, O, M , upper-layered, and lower-layered Na atoms. Surrounding each dopant, there are two nearest $\text{Mn}^{1\text{NN}}$ and four second-nearest $\text{Mn}^{2\text{NN}}$ atoms.

366 meV for the Mg case). The appearance of $(3 - m) \text{Mn}^{4+}$ ions in fully Na-occupied structures indicates that $(4 - m)$ Na ions are immobile and kept in the structure due to the charge conversion. As a result, it is predicted that the overall theoretical capacities of Li- or Mg-doped materials would decrease, which is consistent with the experimental observations [23]. In addition, because of the shorter $\text{Mn}^{4+}-\text{O}$ bonds, the volume of $\text{NaMn}_{15/16}\text{Li}_{1/16}\text{O}_2$ and $\text{NaMn}_{15/16}\text{Mg}_{1/16}\text{O}_2$ structures are significantly smaller than that of the undoped Na_xMnO_2 . Similarly, because Ni dopant prefers the oxidation state of +2 instead of +3 ($E_{\text{NaMn}_{15/16}\text{Ni}_{1/16}^{2+}\text{O}_2} - E_{\text{NaMn}_{15/16}\text{Ni}_{1/16}^{3+}\text{O}_2} = -198$ meV), two Mn^{4+} ions are found at the 2NN sites and the volume of the Ni-doped structure is also smaller than the undoped structure of NaMnO_2 .

When a Mn ion is replaced by a Ti dopant, the Ti ion favorably oxidizes to $4+$ (d^0) while the Mn^{3+} ion at 2NN site would receive an extra electron to become a Mn^{2+} ion ($E_{\text{NaMn}_{15/16}\text{Ti}_{1/16}^{4+}\text{O}_2} - E_{\text{NaMn}_{15/16}\text{Ti}_{1/16}^{3+}\text{O}_2} = -327$ meV). With longer $\text{Mn}^{2+}-\text{O}$ bonds, the volume of the $\text{NaMn}_{15/16}\text{Ti}_{1/16}\text{O}_2$ structure is significantly larger than that of the undoped Na_xMnO_2 .

For the case of Al^{3+} dopants and other transition-metal dopants M^{3+} , all of the Mn ions would keep their oxidation number of 3+. It is found that V^{3+} , Cr^{3+} , and Fe^{3+} ions have preferences in the high spin configurations, whilst Co^{3+} ions should have a low spin configuration. Although the volume of $\text{NaMn}_{15/16}\text{Co}_{1/16}\text{O}_2$ is significantly smaller than the undoped structure due to the shorter $\text{Co}-\text{O}$ bond length, Al, V, and Cr dopants keep the volume almost unchanged. This result can be understood by the $M^{3+}-\text{O}$ bond lengths listed in Table I: The average $M^{3+}-\text{O}$ bond lengths are approximately equal to the average $\text{Mn}^{3+}-\text{O}$ bond lengths.

The lattice distortion degree δ is a parameter to evaluate the cooperative Jahn-Teller distortion (b -axial elongation and a -axial shrinkage) in the lattice of P2-layered oxides [24].

TABLE I. Calculated lattice parameters and average $M-\text{O}$ bond lengths in the $4 \times 2 \times 1$ supercell of $\text{NaMn}_{1-y}\text{M}_y\text{O}_2$ doped-structure supercells ($y = 0.0625$).

Dopants M	a (Å)	b (Å)	c (Å)	V (Å ³)	$M-\text{O}$ (Å)
Undoped	11.46	11.20	10.65	1367.66	2.08
Li^+	11.49	11.01	10.62	1343.23	2.15
Mg^{2+}	11.51	11.07	10.66	1357.50	2.10
Al^{3+}	11.46	11.11	10.70	1367.67	1.97
Ti^{4+}	11.56	11.15	10.67	1374.21	2.02
V^{3+}	11.50	11.15	10.66	1366.20	2.06
Cr^{3+}	11.51	11.15	10.65	1366.83	2.03
Fe^{3+}	11.50	11.14	10.67	1366.63	2.07
Co^{3+}	11.46	11.12	10.65	1357.73	1.98
Ni^{2+}	11.51	11.09	10.65	1359.39	2.12

At $x = 2/3$, the experimental lattice distortion is 8% [24]. Based on the calculated crystal parameters given in Table I, the lattice distortion degrees δ at $x = 1$ can be estimated by using the following equation [24]:

$$\delta = \frac{2b}{a\sqrt{3}} - 1, \quad (1)$$

where a and b are lattice parameters of the supercell along the [100] and [010] directions, respectively. For the undoped structure NaMnO_2 , the lattice distortion is 12.82% at $x = 1$, as shown in Fig. 2. When a Mn ion is replaced by another metal ion, the lattice distortion degree of the doped structure is generally reduced significantly, suggesting that the dopant can help to reduce the large distortion caused by the $\text{Mn}-\text{O}$ bond along the [010] direction. Among M -doped structures, the Li-doped structure has the smallest lattice distortion of 10.64%, followed by the Mg-doped structure (11.09%) due to the shorter $\text{Mn}^{4+}-\text{O}$ bonds in the fully Na-occupied structure. Similarly, the Ni^{2+} dopant also decreases the lattice distortion degree to 11.29% because of the Mn^{4+}O_6 in the structure. Meanwhile, the Ti-doped structure would have a significantly lower lattice distortion degree because it has a larger a lattice parameter due to the long $\text{Mn}^{2+}-\text{O}$ bonds. In addition, significant decreases are witnessed in the lattice distortions up to approximately 12% in the Al-, V-, Cr-, Fe-, and Co-doped structures.

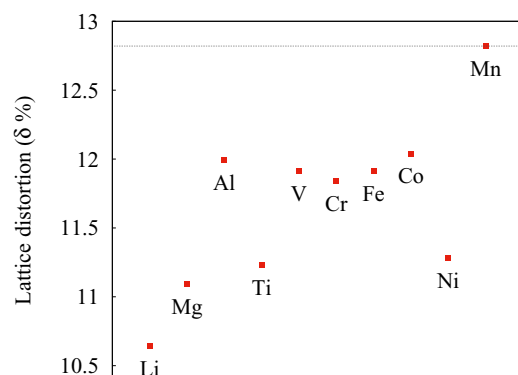


FIG. 2. Lattice distortion degrees of the doped structure $\text{NaMn}_{1-y}\text{M}_y\text{O}_2$ ($y = 0.0625$, $M = \text{Li}, \text{Mg}, \text{Al}, \text{Ti}, \text{V}, \text{Cr}, \text{Fe}, \text{Co}, \text{Ni}$).

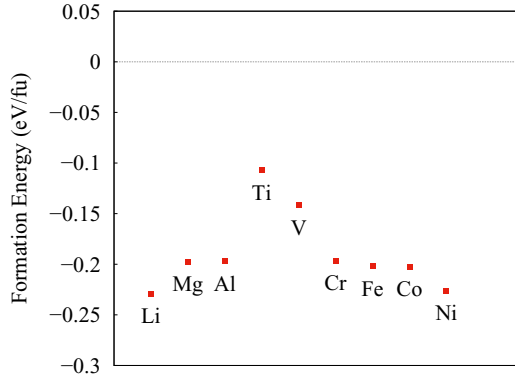
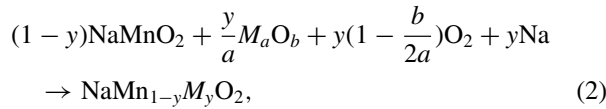


FIG. 3. Formation energies of the doped structure $\text{NaMn}_{1-y}\text{M}_y\text{O}_2$ ($y = 0.0625$, $M = \text{Li, Mg, Al, Ti, V, Cr, Fe, Co, Ni}$).

B. Effect on structure stability

The formation energy of the different phases is used to determine the relative thermal stability with respect to reference structures. Based on the following reactions:



the formation energy can be estimated by the following formula:

$$\Delta H_f = E_{\text{NaMn}_{1-y}\text{M}_y\text{O}_2} - (1-y)E_{\text{NaMnO}_2} - \frac{y}{a}E_{\text{M}_a\text{O}_b} - y\left(1 - \frac{b}{2a}\right)E_{\text{O}_2} - yE_{\text{Na}}, \quad (3)$$

where $y = 1/16$; $E_{\text{NaMn}_{1-y}\text{M}_y\text{O}_2}$, E_{NaMnO_2} , $E_{\text{M}_a\text{O}_b}$, E_{O_2} , and E_{Na} are total energies of $\text{NaMn}_{1-y}\text{M}_y\text{O}_2$, NaMnO_2 , M_aO_b , O_2 , and Na, respectively. M_aO_b is the general chemical formula of oxides and M stands for Li, Mg, Al, Ti, V, Cr, Fe, Co, and Ni. The stable oxides of Li_2O (space group $Fm\bar{3}m$), MgO (space group $Fm\bar{3}m$), Al_2O_3 (space group $R\bar{3}c$), TiO_2 (space group $P4_2/mnm$), V_2O_5 (space group $Pmmn$), Cr_2O_3 (space group $R\bar{3}c$), Fe_2O_3 (space group $R\bar{3}c$), CoO (space group $Fm\bar{3}m$), and NiO (space group $Fm\bar{3}m$) are chosen as references [41]. As can be seen from Fig. 3, the heats of formation of all cationic doped phases are negative, implying that the cationic dopants can be substituted to Mn sites with no phase separation. These results of the formation energy are consistent with experimental features that the synthesized Li-, Mg-, Co-, and Ni-doped structures are stabilized after doping [24].

In previous reports, Li^+ and Mg^{2+} cations can migrate out of the MO_2 layers to become excessive charge carriers in O3 Li-rich phase $\text{Li}[\text{Li}_y\text{M}_{1-y}]\text{O}_2$, which might exacerbate voltage fade [42,43]. In 2020, Eum *et al.* proved that the arrangement of oxygen layers in the O2 phase of $\text{Li}_x(\text{Li}_{0.2}\text{Ni}_{0.2}\text{Mn}_{0.6})\text{O}_2$ can restrict the movements of dopants [44]. To verify if the P2 phase can also restrict the dopants' movement from MnO_2 layers to Na layers, we first compared the total energies of structures in which the lightweight Li and Mg dopants are in the M_{Mn} site of the MnO_2 layer, intermediate M_{inter} site, edge-shared M_e sites, and face-shared M_f sites, as shown in Figs. 4 and 5. Our calculated results indicate that at rich Na concentrations, Li dopants hardly diffuse out

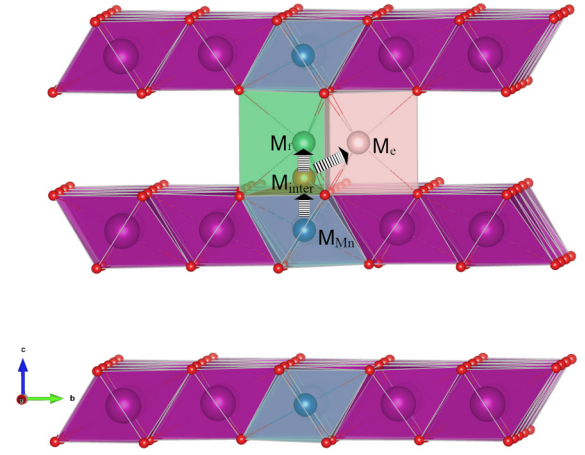


FIG. 4. Dopant's migration path from Mn-layer site (blue balls) to intermediate site (brown ball) and to Na-layer face-shared sites (green ball) or edge-shared site (pink ball). M stands for Li and Mg.

of the MnO_2 layer because of the large energy difference ($E_{\text{Li-at-Mn-site}} - E_{\text{Li-intermediate}} = 1.39 \text{ eV}$) due to the repulsive interaction with Na^+ neighbors. However, at low Na contents, a negative site energy ($E_{\text{Li-at-Mn-site}} - E_{\text{Li-intermediate}}$) of -0.150 eV suggests the structure in which the Li dopant is out of the MnO_2 layer would be significantly more stable. Thus, at low Na content, the Li dopant would prefer to diffuse out of the MnO_2 layer due to its small positive charge and ionic radius. However, this type of dopant would not migrate to the Na_e site or Na_f site because of the very large site energies. Similarly, for the Mg dopant, at low Na concentrations, the Mg^{2+} ion hardly jumps out of the MnO_2 plane with a large energy difference of 1.050 eV due to its charge and ionic size. This result is consistent with the observation from experiments that Mg^{2+} ions remain in the lattice [45]. Therefore, it is expected that the P2 structure can prevent the dopant migration similar to the O2-type structure.

C. Redox potential

The redox potential represents the energy required for a Na atom removal from the fully Na-occupied system. The

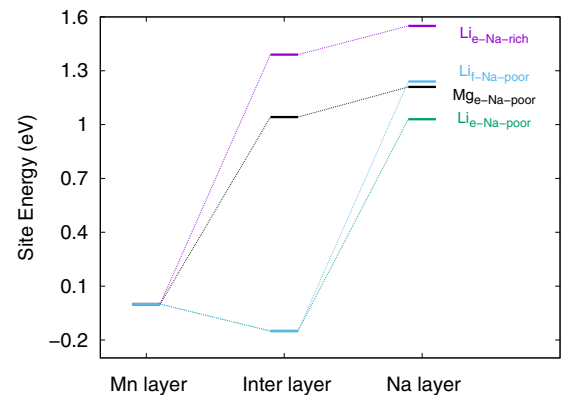


FIG. 5. Relative site energies of structures containing dopants at the Mn-layer site, intermediate site, edge-shared site, and face-shared site in the Na layer calculated along the dopant's migration paths ($M = \text{Li, Mg}$) at rich and poor Na contents.

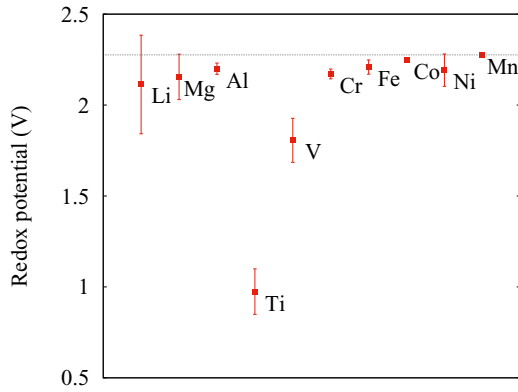


FIG. 6. Redox potentials of doped structures $\text{NaMn}_{1-y}\text{M}_y\text{O}_2$ ($y = 0.0625$, $M = \text{Li, Mg, Al, Ti, V, Cr, Fe, Co, Ni}$).

average redox potential \bar{V} and standard deviation (SD) can be estimated by the following formulas:

$$V_{i-1\text{Na}} = \frac{E_{i-\text{Na}_{31/32}\text{Mn}_{1-y}\text{M}_y\text{O}_2} + E_{\text{Na}} - E_{\text{NaMn}_{1-y}\text{M}_y\text{O}_2}}{xe}, \quad (4)$$

$$\bar{V} = \frac{\sum V_{i-1\text{Na}}}{n}, \quad (5)$$

$$\text{SD} = \sqrt{\frac{\sum (V_{i-1\text{Na}} - \bar{V}_{1\text{Na}})^2}{n-1}}, \quad (6)$$

where $V_{i-1\text{Na}}$ is the redox potential obtained by removing one Na atom at site i . $E_{i-\text{Na}_{31/32}\text{Mn}_{1-y}\text{M}_y\text{O}_2}$, E_{Na} , and $E_{\text{NaMn}_{1-y}\text{M}_y\text{O}_2}$ represent the total energy of the $\text{Na}_{31/32}\text{Mn}_{1-y}\text{M}_y\text{O}_2$ configuration in which the Na vacancy is at site i ; the total energy of Na and $\text{NaMn}_{1-y}\text{M}_y\text{O}_2$, respectively; n is the total number of Na-vacant configurations $\text{Na}_{31/32}\text{Mn}_{1-y}\text{M}_y\text{O}_2$; and $y = 1/16$. M stands for Li, Mg, Al, Ti, V, Cr, Fe, Co, and Ni. The average redox potentials of different doped structures with SD are demonstrated in Fig. 6. It is found that the structures containing Li, Mg, Al, Cr, Fe, Co, and Ni dopants exhibit similar average redox potentials as compared with the undoped NaMnO_2 . This point is consistent with experimental data [24]. However, the Ti and V dopants reduce the redox potentials at high Na content and facilitate the Na deintercalation. In addition, the SD of redox potentials in Li, Mg, Ti, V, and Ni cases are significantly large, implying the total energies of the structures having one Na vacancy at different sites are substantially dependent on the distances between Na vacancy and the dopants. Indeed, in the Li-, Mg-, and Ni-doped structures, Na vacancy is preferably at the site near the dopants because it helps to reduce repulsion between positive ions around these dopants, which are often surrounded by Mn^{4+}O_6 octahedra.

D. Electronic structures

To build our grasp of the electronic structures and to interpret the effects of dopants on the redox potentials, the density of states (DOS) of the doped systems are calculated. The DOS of the undoped NaMnO_2 and doped system $\text{NaMn}_{1-y}\text{M}_y\text{O}_2$ are illustrated in Fig. 7. In all the DOS figures, the Fermi levels are set at the highest occupied states of the valence bands (VBs). As mentioned above, the Ti or V dopants reduce the redox potentials compared with that of NaMnO_2 . For the

Ti and V- cases, the Fermi levels shift toward the conduction band (CB) by 1.19 eV and 0.51 eV, respectively, suggesting the significant increases in the electron chemical potentials. Thus, it facilitates the Na extraction. The Fermi level shifting toward the CB is a good explanation for the lower redox potential of the Ti- and V-doped materials. Moreover, in the Ti-doped case, the appearance of Mn^{2+} occupied states right below the Fermi level results in the narrower band gap of 1.54/4.39 eV. Consequently, when a Na atom is extracted, electrons at these states may jump first to a newborn polaron state in the band gap with a considerably small energy. Similarly, for the V-doped case, the occupied 3d V^{3+} states are distributed into the highest energy region below the Fermi level, and then V^{3+} would be oxidized first to be V^{4+} . These V occupied states right below the Fermi level also truncate the band gap to 2.36/4.73 eV as well.

By contrast, the Fermi level of the fully Na-occupied structures does not shift much if substituting Mn by the Li, Mg, Al, Cr, Fe, Co, and Ni dopants, so the significant reduction in the redox potentials of these doped systems is hardly observed. Among these dopants, Al, Cr, Fe, and Co dopants slightly increase the up-/down-spin band gap to 2.83/4.76 eV, 2.77/4.71 eV, 2.83/3.86 eV, 2.72/4.33 eV, respectively, while the Li, Mg, and Ni dopants significantly reduce the up-/down-spin band gap to 2.23/4.24 eV, 2.11/4.35 eV, and 2.16/4.14 eV, respectively, due to the newborn Mn^{4+} unoccupied states appearing at the CB bottom. Because the states induced by dopants to DOS are far from the Fermi level while the states near the Fermi level originate mainly by hybridization of 3d Mn^{3+} states and 2p O states, Mn^{3+} ions are likely to be oxidized first to be Mn^{4+} when a Na atom is removed, and the 3d states of Mn^{3+} ions would mainly determine the electronic property of these doped materials of a small dopant's contents. This is consistent with the previous mechanism observed from several experiments of layered oxides, in which Mn^{3+} ions would be oxidized first [46]. Therefore, it provides evidence to explain why the Li-, Mg-, Al-, Cr-, Fe-, Co-, and Ni-doped structures exhibit redox potentials similar to the undoped NaMnO_2 .

E. Effect on diffusion mechanism

To get deeper insight into the ionic conductivity, the diffusion mechanism of the Na ion is explored extensively. With the cathode materials based on transition metals, a quasiparticle, called the small polaron, is formed at transition metal sites and simultaneously accompanies the Na ion diffusion. As indicated in our previous report [20], the positive polaron may form at the third-nearest-neighbor Mn site (3NN) at high sodium concentrations. The activation energy for the accompanying polaron–Na ion complex is 518 meV at rich Na regimes and tends to reduce to 327 meV at poor Na regimes. It is also noted that the polaron can jump in plane or interplane of MnO_2 layers with the same activation energy. Since the effect of polaron migration between crossing and parallel processes is equivalent, we concentrate on the doping effect of other metals on Na diffusion. In addition, because the activation energy is higher at high Na concentrations, only the Na ion-accompanying polaron complex diffusion near the dopant's site at rich Na regimes are considered, which the Na

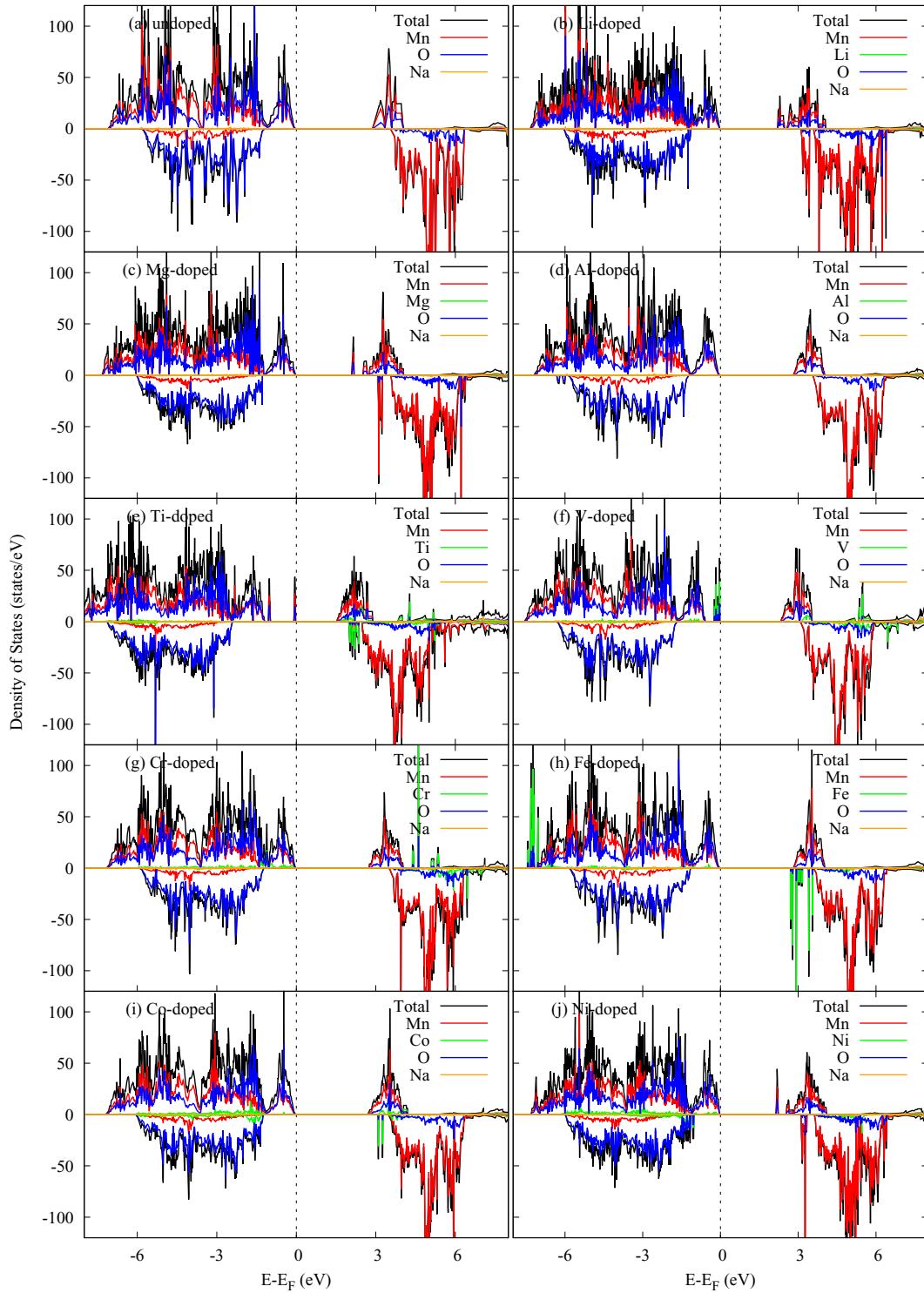


FIG. 7. Density of states of doped structures $\text{NaMn}_{1-y}\text{M}_y\text{O}_2$ where $y = 0.0625$ and M stands for Li, Mg, Al, Ti, V, Cr, Fe, Co, and Ni. The Fermi levels are set at the highest occupied states of the valence band.

vacancy would diffuse from the A site to the B site, as can be seen from Fig. 8.

1. Ti dopants

We investigate the Ti-doping effect on the diffusion of Na ions at three Na concentrations ($x = 31/32, 30/32,$ and

$29/32$). As indicated in the previous section, at $y = 1$, the Ti dopants induce the appearance of Mn^{2+} ions and the localized states of Mn^{2+} ions located near the Fermi level would preferably be oxidized first. The localized states and local distortion due to the longer bond lengths of Mn^{2+}O_6 octahedra provide stringent proof of the negative polaron at Mn^{2+} ions. When one Na ion is deintercalated from the full

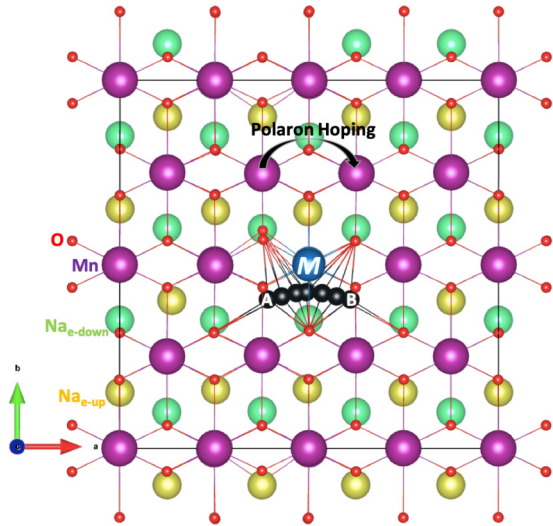


FIG. 8. Diffusion path of a Na ion near the dopants. Green, yellow, red, purple, blue, and black balls represent Na atoms at lower layer and upper layer, O, Mn, dopant M, and Na-vacancy trace. A and B stand for the initial and final position of Na ion for diffusion. The arrow indicates the polaron hopping between two adjacent Mn sites.

occupied structure $[(1-x) = 1/32 < y = 2/32$, monovacancy], one Mn^{2+} ion would become Mn^{3+} so the negative polaron at this site disappears while another negative polaron is found in another Mn^{2+} site of the structure. This negative polaron can be traced since the local bound state is located near the Fermi level, as shown in Fig. 9(a). The diffusion of the Na ion accompanied by the negative polaron in the neighborhood of TiO_6 octahedron at high Na regimes is investigated. Our NEB calculations indicate that the activation energy for diffusion of the Na ion-accompanying polaron complex under the Ti^{4+}O_6 environment is 447 meV with a reaction coordinate of 3.4 Å.

At $(1-x) = y = 2/32$ (di-Na vacancy), one more Na ion is deintercalated from the structure. In this case, all the Mn ions would keep an oxidation number of +3 while all the Ti-dopant ions have the oxidation number of +4. DOS of the most stable of $\text{Na}^+/\text{Mn}^{3+}/\text{M}^{4+}$ ordering is illustrated in Fig. 9(c). No local bound state suggests that no small polaron may form at this concentration. The Na ion diffusion between two edge-share sites near the TiO_6 environment without the polaron effect is demonstrated in Fig. 9(d). In this case, the activation energy for the diffusion of the Na ion slightly increases to 487 meV with a reaction coordinate of 3.0 Å.

At $y < (1-x) = 3/32$ (tri-Na vacancy), one more Na ions is deintercalated from the structure. As a result, one Mn^{3+} ion would be oxidized to be Mn^{4+} , which causes the bound states appearing at the bottom of the CB, as illustrated in Fig. 9(e). This local state provides evidence of a positive polaron formed at $\text{Mn}^{3\text{NN}}$ transition metal sites. Our NEB calculation shown in Fig. 9(f) points out that, when the diffusion of the Na ion-positive polaron complex between two edge-share sites near the TiO_6 sites takes place, an activation energy of 555 meV is required for the Na vacancy-positive polaron complex diffusion.

2. V dopants

For the V case, the states on the VB top are mainly contributed by V's 3d states. Therefore, when a Na atom is deintercalated from the fully Na occupied system $\text{NaMn}_{1-y}\text{V}_y\text{O}_2$ ($y = 1/16$), one V^{3+} remains its oxidation number while another V^{3+} ion is oxidized to V^{4+} . As can be seen from Fig. 10(a), one bound state at the CB bottom of V^{4+} provides the evidence for positive polaron forming at the V^{4+} site in the structure. The single process, in which the positive polaron preferably sits at the V^{4+}O_6 octahedron and Na vacancy diffuses in the space between V^{4+}O_6 and V^{3+}O_6 octahedra, was investigated. The energy profile of this process is illustrated in Fig. 10(b). The energy barrier of Na ion diffusion is 455 meV with a reaction coordinate of 2.95 Å.

At $y = (1-x) = 1/16$ (di-Na vacancy), another Na ion is removed from the one-Na-vacant structure. All of Mn ions would hold the oxidation number of +3 (d^4) while all the V dopant ions keep the oxidation number of +4 (d^1). DOS of the most stable $\text{Na}^+/\text{Mn}^{3+}/\text{M}^{4+}$ ordering are shown in Fig. 10(c). In this case, the states originated from the 3d V electrons in the CB bottom imply that two small polarons form in $\text{Na}_{1/16}\text{V}_{1/16}\text{Mn}_{15/16}\text{O}_2$ due to di-Na vacancy. As a sequence, the diffusion of Na ion requires a higher activation energy of 563 meV with a reaction coordinate of 2.91 Å in comparison with a single Na vacancy case.

At $y < (1-x) = 3/32$ (tri-Na vacancy), one more Na ion is removed. Similar to the Ti case, one Mn^{3+} ion is oxidized to Mn^{4+} . A hole state from such a Mn^{4+} ion appearing right below the CB bottom provides evidence of a new positive polaron forming at the $\text{Mn}^{3\text{NN}}$ site. The activation energy for the diffusion of the Na ion-positive polaron complex between two edge-share sites near the VO_6 sites is 467 meV, as indicated in Fig. 10(f).

3. Other dopants ($M = \text{Li, Mg, Al, Cr, Fe, Co, Ni}$)

For dopants such as Li, Mg, Al, Cr, Fe, Co, and Ni, because the hybridized states between 3d Mn^{3+} and 2p O states predominantly determine the electrochemical properties of the doped materials, when a Na vacancy is introduced into the fully Na-occupied structure, the Mn^{3+} atom is oxidized to Mn^{4+} preferably. The local states appearing below the CB bottom suggest a positive polaron forming at Mn^{4+} , as indicated in the Supplemental Material [47]. The diffusion of Na vacancy from the A to B sites in the environment of MO_6 octahedra during the positive polaron migrates from the Mn_A to Mn_B sites are shown in Fig. 8.

Table II summarizes the parameters derived from NEB calculations, including dopant charges Q , absolute bond lengths d_{M-O} , reaction coordinates, activation energies E_a , and diffusivities D . The absolute bond length change (Å) is defined by the following formula:

$$\delta d_{M-O} = \sum_{i=1}^6 |d_{M-O_i}^{\text{initial}} - d_{M-O_i}^{\text{final}}|, \quad (7)$$

where $d_{M-O_i}^{\text{initial}}$, $d_{M-O_i}^{\text{final}}$ are bond lengths of dopants with six surrounding oxygens in the initial and final states. The diffusivity can be estimated from the Einstein-Smoluchowski relation,

$$D = v^* d^2 e^{-E_a/k_B T}, \quad (8)$$

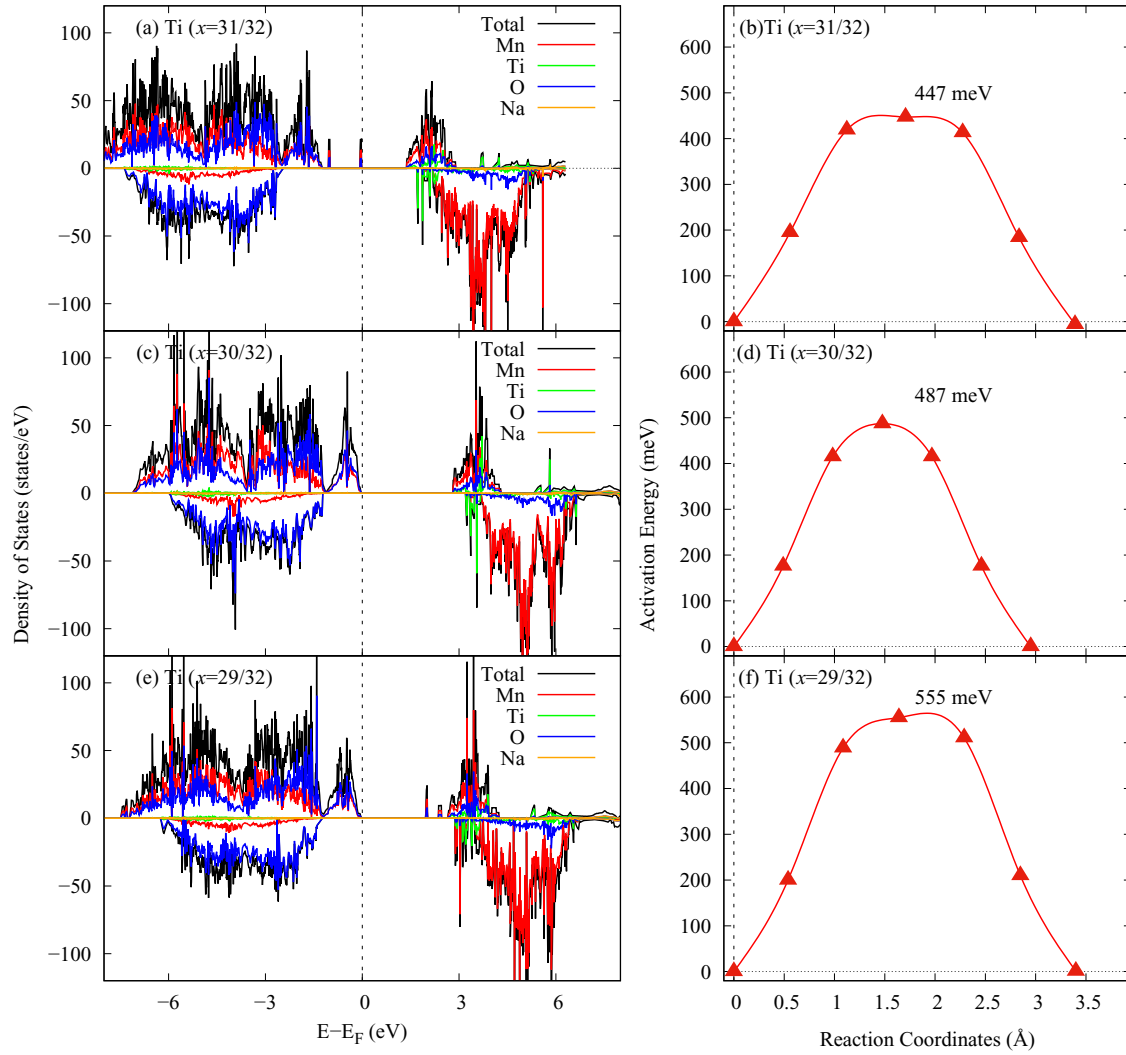


FIG. 9. Density of states and activation energy profiles for diffusion of Na ion-accompanying polaron complex at different Na concentrations of $\text{Na}_x\text{Mn}_{15/16}\text{Ti}_{1/16}\text{O}_2$ ($29/32 \leq x \leq 31/32$).

where v^* is assumed to be $5 \times 10^{12} \text{ s}^{-1}$ [48] and d is the distance of Na ion diffusion. E_a is the activation energy, $T = 300 \text{ K}$, and k_B is Boltzmann constant ($k_B = 8.617 \times 10^{-5} \text{ eV/K}$). It can be seen from Table II that Fe, Mg, Cr dopants hinder the Na ion-positive polaron complex diffusion with significantly higher activation energies of 605, 574, 553 meV,

TABLE II. Dopant charges Q , the absolute bond length changes δd_{M-O} , reaction coordinates E_a , activation energies, and diffusivities D of Na ion diffusion under the dopant's environments.

Dopants	Charge Q	δd_{M-O}	Re-Coor (Å)	E_a (meV)	D (cm^2/s)
Fe	+3	0.304	3.542	605	4.30×10^{-13}
Mg	+2	0.212	3.605	574	1.32×10^{-12}
Cr	+3	0.194	3.419	553	3.00×10^{-12}
Al	+3	0.245	3.470	525	9.12×10^{-12}
Undoped	+3	0.203	3.542	518	1.15×10^{-11}
Ni	+2	0.192	3.601	473	7.34×10^{-11}
Li	+1	0.492	3.453	442	2.23×10^{-10}
Co	+3	0.175	3.329	412	6.64×10^{-10}

respectively, while the Al dopant increases the activation energy by an ignorable amount of 7 meV in comparison with that of the Na ion diffusion in NaMnO_2 (518 meV). As a result, the diffusivities would decrease in these doped systems. By contrast, Li, Co, and Ni dopants benefit from such complex diffusion with a much lower activation energy of 442, 412, and 473 meV, respectively, so the ionic diffusivities would increase significantly. Because the polaron hops between two neighboring MnO_6 octahedra, the influence of the doping on the activation energy of the Na ion-polaron complex can be explained by the work associated with polaron hopping, which is defined by the product of charge Q and the absolute bond length change: $W_{\text{polaron-hopping}} = \delta d_{M-O} \times Q$. It is found that dopants with a smaller positive charge like Li^+ or small average $M-O$ bond length changes, such as Co^{3+}O_6 , may benefit from the Na ion diffusion. Therefore, we point out that the higher the works associated with polaron hopping, the lower the activation energies. In other words, the activation energies of Na ion-positive polaron complex diffusion near the dopant octahedron are strongly affected by the charge of dopants and bond $M-O$ vibration.

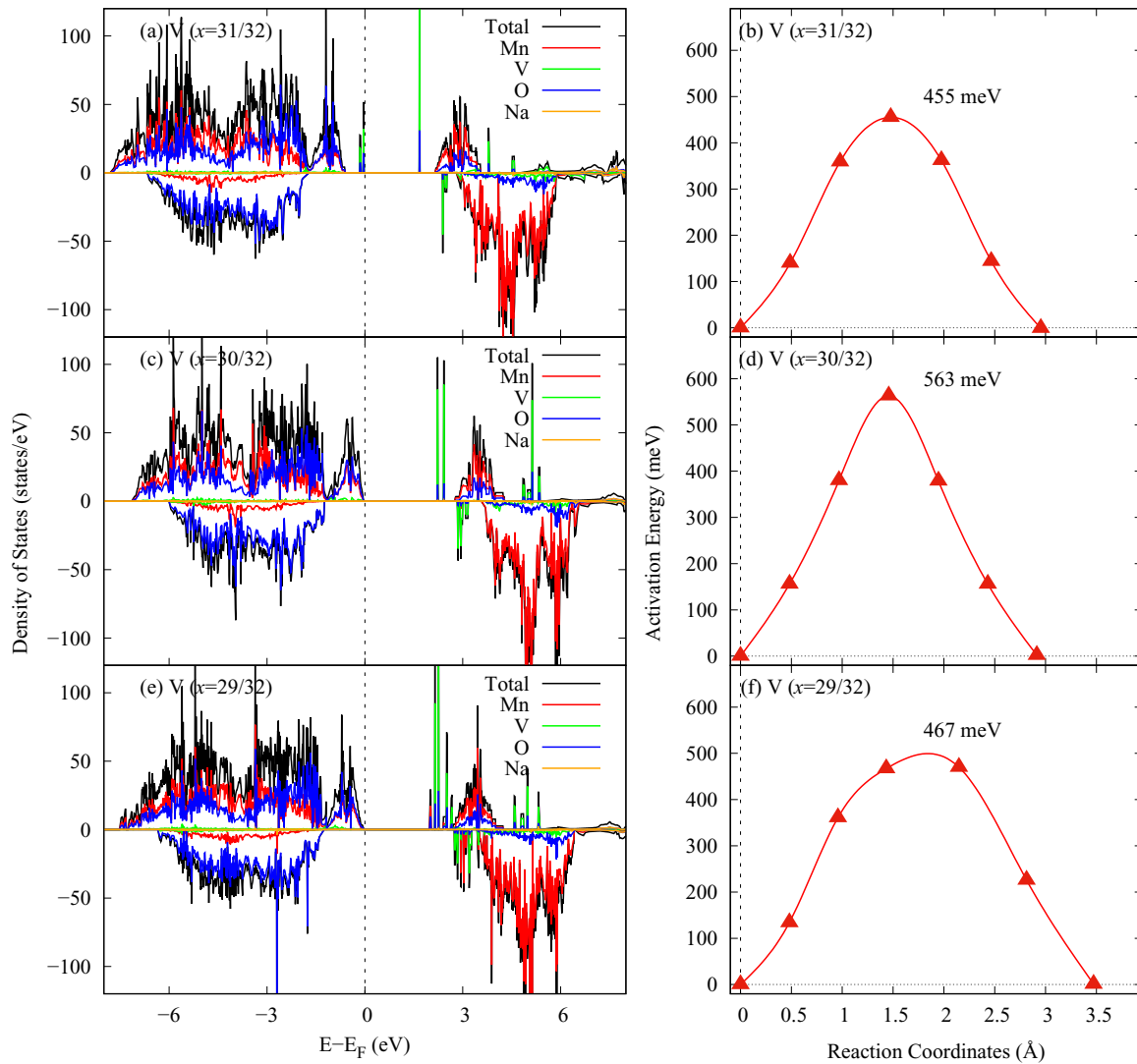


FIG. 10. Density of states and activation energy profiles for diffusion of Na ion-accompanying polaron complex at different Na concentrations of $\text{Na}_x\text{Mn}_{15/16}\text{V}_{1/16}\text{O}_2$ ($29/32 \leq x \leq 31/32$).

IV. CONCLUSIONS

In conclusion, we have systematically reported the doping effect of Li, Mg, Al, Ti, V, Cr, Fe, Co, Ni dopants on the electrochemical properties of a promising layered oxide NaMnO_2 in the aspect of lattice distortion, stability, redox potential, and Na ion-polaron complex diffusion using the HSE06 method. It is found that all dopants reduce the lattice distortion, especially in Li-, Mg-, Ti-, and Ni-doping cases. In addition, all dopants increase the stability of the structure in the particular cases of Ti, Al, and V. However, it is found that in the fully Na-occupied systems, Ti and V dopants significantly reduce the redox potential while other dopants exhibit a small influence on the redox potential. Regarding the doping effect on the diffusion of a Na ion-polaron complex, it is found that Fe, Mg, Cr, and Ti dopants hinder the Na ion-positive polaron complex diffusion with significantly higher activation energies of 605 meV, 574 meV, 555 meV, and 553 meV, respectively. As a result, the diffusivity decreases in systems containing these dopants. For the Al dopant, the activation

energy almost kept its value as in the pure system. In contrast, Li, V, Co, and Ni dopants benefit from such complex diffusion with a much lower activation energy of 442, 467, 412, and 473 meV, respectively, resulting in the significant increase of the ion diffusivity. Based on these findings, we can expect that Li, V, Co, and Ni dopants can improve the electrochemical properties of the promising layered oxide NaMnO_2 .

ACKNOWLEDGMENTS

This work was supported by the Japanese Government Scholarship from the Ministry of Education, Culture, Sports, Science and Technology (MEXT), Japan and the ESICB project (Grant No. JPMXP0112101003) of MEXT, Japan. The numerical calculations of this paper were performed using a supercomputer at the Institute for Solid State Physics, University of Tokyo. The authors would like to acknowledge Koun Shirai and Kunihiko Yamauchi for their valuable comments.

- [1] V. Palomares, P. Serras, I. Villaluenga, K. B. Hueso, J. Carretero-González, and T. Rojo, *Energy Environ. Sci.* **5**, 5884 (2012).
- [2] M. D. Slater, D. Kim, E. Lee, and C. S. Johnson, *Adv. Funct. Mater.* **23**, 947 (2013).
- [3] H. Pan, Y.-S. Hu, and L. Chen, *Energy Environ. Sci.* **6**, 2338 (2013).
- [4] J.-Y. Hwang, S.-T. Myung, and Y.-K. Sun, *Chem. Soc. Rev.* **46**, 3529 (2017).
- [5] B. Dunn, H. Kamath, and J.-M. Tarascon, *Science* **334**, 928 (2011).
- [6] N. Yabuuchi, K. Kubota, M. Dahbi, and S. Komaba, *Chem. Rev.* **114**, 11636 (2014).
- [7] S. Y. Lim, H. Kim, R. Shakoor, Y. Jung, and J. W. Choi, *J. Electrochem. Soc.* **159**, A1393 (2012).
- [8] Y.-U. Park, D.-H. Seo, H. Kim, J. Kim, S. Lee, B. Kim, and K. Kang, *Adv. Funct. Mater.* **24**, 4603 (2014).
- [9] J. Song, L. Wang, Y. Lu, J. Liu, B. Guo, P. Xiao, J.-J. Lee, X.-Q. Yang, G. Henkelman, and J. B. Goodenough, *J. Am. Chem. Soc.* **137**, 2658 (2015).
- [10] L. Wang, Y.-G. Sun, L.-L. Hu, J.-Y. Piao, J. Guo, A. Manthiram, J. Ma, and A.-M. Cao, *J. Mater. Chem. A* **5**, 8752 (2017).
- [11] X. Chen, X. Zhou, M. Hu, J. Liang, D. Wu, J. Wei, and Z. Zhou, *J. Mater. Chem. A* **3**, 20708 (2015).
- [12] M. Hamaguchi, H. Momida, and T. Oguchi, *J. Phys. Soc. Jpn.* **87**, 044805 (2018).
- [13] A. Kitajou, H. Momida, T. Yamashita, T. Oguchi, and S. Okada, *ACS Appl. Energy Mater.* **2**, 5968 (2019).
- [14] H. Kotaka, H. Momida, A. Kitajou, S. Okada, and T. Oguchi, *Chem. Rec.* **19**, 811 (2019).
- [15] M. Hamaguchi, H. Momida, A. Kitajou, S. Okada, and T. Oguchi, *Electrochi. Acta* **354**, 136630 (2020).
- [16] H. Momida, A. Kitajou, S. Okada, and T. Oguchi, *J. Phys. Soc. Jpn.* **88**, 124709 (2019).
- [17] T. Yamashita, H. Momida, and T. Oguchi, *Electrochi. Acta* **195**, 1 (2016).
- [18] A. Caballero, L. Hernan, J. Morales, L. Sanchez, J. Santos Pena, and M. A. G. Aranda, *J. Mater. Chem.* **12**, 1142 (2002).
- [19] S. Kumakura, Y. Tahara, K. Kubota, K. Chihara, and S. Komaba, *Angew. Chem., Int. Ed.* **55**, 12760 (2016).
- [20] H. D. Luong, V. A. Dinh, H. Momida, and T. Oguchi, *Phys. Chem. Chem. Phys.* **22**, 18219 (2020).
- [21] V. A. Dinh, J. Nara, and T. Ohno, *Appl. Phys. Express* **5**, 045801 (2012).
- [22] J. Billaud, G. Singh, A. R. Armstrong, E. Gonzalo, V. Roddatis, M. Armand, T. Rojo, and P. G. Bruce, *Energy Environ. Sci.* **7**, 1387 (2014).
- [23] M.-S. Kwon, S. G. Lim, Y. Park, S.-M. Lee, K. Y. Chung, T. J. Shin, and K. T. Lee, *ACS Appl. Mater. Interfaces* **9**, 14758 (2017).
- [24] S. Kumakura, Y. Tahara, K. Kubota, K. Chihara, and S. Komaba, *Chem. Mater.* **29**, 8958 (2017).
- [25] C. Zheng, B. Radhakrishnan, I.-H. Chu, Z. Wang, and S. P. Ong, *Phys. Rev. Appl.* **7**, 064003 (2017).
- [26] K. M. Bui, V. A. Dinh, and T. Ohno, *Appl. Phys. Express* **5**, 125802 (2012).
- [27] K. M. Bui, V. A. Dinh, and T. Ohno, *J. Phys.: Conf. Ser.* **454**, 012061 (2013).
- [28] D. M. Duong, V. A. Dinh, and T. Ohno, *Appl. Phys. Express* **6**, 115801 (2013).
- [29] K. M. Bui, V. A. Dinh, S. Okada, and T. Ohno, *Phys. Chem. Chem. Phys.* **17**, 30433 (2015).
- [30] K. M. Bui, V. A. Dinh, S. Okada, and T. Ohno, *Phys. Chem. Chem. Phys.* **18**, 27226 (2016).
- [31] M. Debbichi, L. Debbichi, V. A. Dinh, and S. Lebegue, *J. Phys. D: Appl. Phys.* **50**, 045502 (2016).
- [32] T. L. Tran, H. D. Luong, D. M. Duong, N. T. Dinh, and V. A. Dinh, *ACS Omega* **5**, 5429 (2020).
- [33] H. D. Luong, T. D. Pham, Y. Morikawa, Y. Shibutani, and V. A. Dinh, *Phys. Chem. Chem. Phys.* **20**, 23625 (2018).
- [34] H. D. Luong, V. A. Dinh, H. Momida, and T. Oguchi, *J. Alloy. Compd.* **875**, 159963 (2021).
- [35] G. Kresse and J. Hafner, *Phys. Rev. B* **49**, 14251 (1994).
- [36] J. P. Perdew, K. Burke, and M. Ernzerhof, *Phys. Rev. Lett.* **77**, 3865 (1996).
- [37] J. Heyd, G. E. Scuseria, and M. Ernzerhof, *J. Chem. Phys.* **118**, 8207 (2003).
- [38] M. Aykol, S. Kim, and C. Wolverton, *J. Phys. Chem. C* **119**, 19053 (2015).
- [39] S. Grimme, S. Ehrlich, and L. Goerigk, *J. Comput. Chem.* **32**, 1456 (2011).
- [40] D. Sheppard, P. Xiao, W. Chemelewski, D. D. Johnson, and G. Henkelman, *J. Chem. Phys.* **136**, 074103 (2012).
- [41] A. Jain, S. P. Ong, G. Hautier, W. Chen, W. D. Richards, S. Dacek, S. Cholia, D. Gunter, D. Skinner, G. Ceder, and K. A. Persson, *APL Mater.* **1**, 011002 (2013).
- [42] K. Ku, J. Hong, H. Kim, H. Park, W. M. Seong, S.-K. Jung, G. Yoon, K.-Y. Park, H. Kim, and K. Kang, *Adv. Energy Mater.* **8**, 1800606 (2018).
- [43] J.-L. Shi, J.-N. Zhang, M. He, X.-D. Zhang, Y.-X. Yin, H. Li, Y.-G. Guo, L. Gu, and L.-J. Wan, *ACS Appl. Mater. Interfaces* **8**, 20138 (2016).
- [44] D. Eum, B. Kim, S. J. Kim, H. Park, J. Wu, S.-P. Cho, G. Yoon, M. H. Lee, S.-K. Jung, Y. Wanli, W. M. Seong, K. Ku, O. Tamwattana, S. K. Park, I. Hwang, and K. Kang, *Nat. Mater.* **19**, 419 (2020).
- [45] U. Maitra, R. A. House, J. W. Somerville, N. Tapia-Ruiz, J. G. Lozano, N. Guerrini, R. Hao, K. Luo, L. Jin, M. A. Pérez-Osorio, F. Massel, M. P. David, R. Silvia, X. Lu, D. E. McNally, A. V. Chadwick, F. Giustino, T. Schmitt, L. C. Duda *et al.*, *Nat. Chem.* **10**, 288 (2018).
- [46] J. U. Choi, J. H. Jo, Y. J. Park, K.-S. Lee, and S.-T. Myung, *Adv. Energy Mater.* **10**, 2001346 (2020).
- [47] See Supplemental Material at <http://link.aps.org/supplemental/10.1103/PhysRevMaterials.6.015802> for the density of states of the defect structures with a Na vacancy $\text{Na}_{31/32}\text{Mn}_{1-y}\text{M}_y\text{O}_2$ ($M = \text{Li, Mg, Al, Cr, Fe, Co, Ni}$, and $y = 1/16$). The Fermi levels are set at the highest occupied states of the valence bands.
- [48] G. K. P. Dathar, D. Sheppard, K. J. Stevenson, and G. Henkelman, *Chem. Mater.* **23**, 4032 (2011).